Quaternary Science Reviews 212 (2019) 164–177

Contents lists available at ScienceDirect

Quaternary Science Reviews

journal homepage: www.elsevier.com/locate/quascirev

Staged fine-grained sediment supply from the Himalayas to the Bengal Fan in response to climate change over the past 50,000 years

Jianguo Liu [a, b, *], Wei He [a, d], Li Cao [a, d], Zhu Zhu [a, d], Rong Xiang [a], Tiegang Li [b, c, d, **], Xuefa Shi [b, c], Shengfa Liu [b, c]

[a] Key Laboratory of Ocean and Marginal Sea Geology, South China Sea Institute of Oceanology, Chinese Academy of Sciences, Guangzhou, 510301, China
[b] Laboratory for Marine Geology, Qingdao National Laboratory for Marine Science and Technology, Qingdao, 266061, China
[c] Key Laboratory of Marine Sedimentology and Environmental Geology, First Institute of Oceanography, Ministry of Natural Resources, Qingdao, 266061, China
[d] University of Chinese Academy of Sciences, Beijing, 100049, China

ARTICLE INFO

Article history:
Received 29 December 2018
Received in revised form
24 March 2019
Accepted 6 April 2019
Available online 15 April 2019

Keywords:
Sediment provenance
Heinrich events
Sea-level fluctuation
Northeastern indian ocean
Last glacial maximum
Clay minerals
Grain size
Sr and Nd isotopes
Fine-grained sediment

ABSTRACT

The Bengal Fan, as the largest submarine fan in the world, receives a large amount of sediments discharged from the Himalayas through the Ganges-Brahmaputra (G-B) river system. However, previous studies of this system seldom focused on the role of channels, which are widely developed in the Bengal Fan, in sediment transportation over the last glacial cycle. Here, we discuss the coupled sedimentary archive in two gravity cores along the Active Channel in the Bengal Fan. Our findings are based on grain size, clay minerals, and Sr and Nd isotope compositions of these two sediment cores. End-member modeling of grain-size data reveals that the intermediate end-member represents the flux of distal fluvial particles from the G-B river system, the fine end-member denotes regional sediment supply of weathered volcanic materials, especially from the eastern Indian Peninsula, and the coarse end-member probably reflects nearby terrigenous input, aeolian input and/or volcanic glass. Sediment provenance analysis based on clay minerals, and Sr and Nd isotopes confirmed sediment supply from the G-B river system which was characterized by high illite percentage, high $^{87}Sr/^{86}Sr$ ratios and low ε_{Nd} values, especially during five stages (50–45 ka, 42–37 ka, 31–28.5 ka, 24–20 ka and 14–9 ka). During these stages, heavy fine-grained sediment supply from the G-B river system was discharged into the study area under the influence of climate change rather than sea-level fluctuation, additionally emphasizing the importance of channels in the sediment transport process. Moreover, we find a significant alteration of sediment sources at ~26 ka, which may be related to conversion of the deep-water currents in the Bay of Bengal.

1. Introduction

As a result of the India-Asia collision and uplift of the Himalayas and Tibetan Plateau, the Bengal Fan presently receives large amounts of sediments mainly supplied by the Ganges-Brahmaputra (G-B) Rivers, with minor contributions from other rivers in Bangladesh, India and Burma. Currently, the G-B river system, as the world's largest sediment dispersal system, annually discharges 1060 million tons of sediments into the Bay of Bengal (BoB) to the north, together with sediment supply from the Mahanadi (61 million tons annually), Godavari (170 million tons) and Krishna Rivers (64 million tons) to the northwest and the Irrawady (360 million tons) and Salween (180 million tons) Rivers (discharged into the Andaman Sea) to the northeast (Milliman and Farnsworth, 2011). Today, approximately 30% of the sediments exported from the Himalayas are delivered to the Bengal Fan (Goodbred and Kuehl, 1999, 2000). In particular, from June to September, 90% of the annual Ganges River sediments and more than 80% of the Brahmaputra River sediments are transferred during the summer monsoon (Unger et al., 2003). All these fluvial sediments are dispersed by ocean currents and then deposited in deep-water

* Corresponding author. Key Laboratory of Ocean and Marginal Sea Geology, South China Sea Institute of Oceanology, Chinese Academy of Sciences, Guangzhou, 510301, China.
** Corresponding author. University of Chinese Academy of Sciences, Beijing, 100049, China.
E-mail addresses: jgliu@scsio.ac.cn (J. Liu), tgli@fio.org.cn (T. Li).

https://doi.org/10.1016/j.quascirev.2019.04.008
0277-3791/

environments (Colin et al., 1999; Stoll et al., 2007; Awasthi et al., 2014).

In the lower latitude of the BoB, the monsoon current flows eastward in summer but westward in winter (Shankar et al., 2002). In the BoB, the East India Coastal Current (EICC) reverses direction twice a year, and it flows northeastward from February to September with a peak in March–April and southwestward from October to January with the strongest intensity in November (Schott and McCreary, 2001).

The Bengal Fan, as the largest submarine fan in the world, has a length of approximately 3000 km and a width of approximately 1000 km, with a maximum thickness of 16.5 km. A series of channels have developed in the Bengal Fan from outside of the G-B river mouth to the equatorial sea area. Within the fan valley system, channels migrated when sedimentation rates accelerated in the upper and upper middle fan (Curray et al., 2003). The Active Channel (also named the Active Valley) is the most important because it appears to be the only valley cut off from a direct supply of sediment from the rivers and is directly connected to the contemporary submarine canyons.

Previous studies showed that Sr and Nd isotopic compositions (Ahmad et al., 2005; Colin et al., 2006; Joussain et al., 2016) combined with clay minerals in sediments of the surrounding sources of the BoB were distinguished from each other (Venkatar and Biscaye, 1973; Kolla et al., 1976), and their distribution patterns in marine sediments were predominantly controlled by the provenance, sedimentary environment and mineralogical characteristics (Farmer et al., 2003; Ehlert et al., 2013; Stewart et al., 2016); therefore Sr and Nd isotopic compositions were utilized for sediment provenance in the northeastern Indian Ocean (Li et al., 2017). Siliciclastic grain-size data were further utilized to constrain sediment transport dynamics (Paterson and Heslop, 2015; Yu et al., 2018) during the source-to-sink process of sediments from large rivers into the Bengal Fan. In this study, high-resolution investigations of the clay mineralogy, grain-size and Sr and Nd isotopic compositions have been conducted on two deep-sea gravity cores along the Active Channel in the lower Bengal Fan to better trace the variability of sediment sources over the past 50 ka and the implications of fluvial input, climate change and sea-level fluctuation.

2. Materials and methods

Two gravity cores, YDY09 (9°59.611′N, 85°57.659′E, water depth of 3520 m) and 12I712 (4°0.329′N, 82°30.196′E, water depth of 4181 m), were collected by *R/V Shiyan 1* of the South China Sea Institute of Oceanology (SCSIO), Chinese Academy of Sciences (CAS) from the lower Bengal Fan, with one located inside the BoB and the other outside the BoB (Fig. 1). Both cores, YDY09 (with a total length of 244 cm) and 12I712 (with a total length of 261 cm), consisted of gray to green silty clay and were subsampled at 1 cm intervals for grain-size and clay mineral determination, and some samples were further analyzed for Sr and Nd isotope measurements.

The sediment samples were treated with excess H_2O_2 (10%), followed by treatment with an excess of HCl (10%), to remove organic material and carbonates, respectively, and then repeatedly rinsed three times with deionized H_2O and centrifuged. The grain-size distribution of the terrigenous fraction was measured with a Malvern Mastersizer 2000 at the SCSIO, CAS. This instrument can analyze grains in the 0.02–2000 μm range. The measurement repeatability is 0.5% for a single sample, and the reproducibility is better than 2% for duplicate samples.

After removing organic materials and carbonate using 10% hydrogen peroxide (H_2O_2) and 10% acetic acid (CH_3COOH), respectively, the sediment samples were separated for clay mineral (<2 μm) differentiation according to Stokes' settling velocity principle. Subsequently, the oriented glass with clay minerals was measured by standard X-ray diffraction (XRD) using a D8 ADVANCE diffractometer with CuKα radiation at the Key Laboratory of Marine Geology and Environment, Institute of Oceanology, CAS. The clay mineralogy determination was based primarily on the position of the (001) series of basal reflections on the XRD diagram of the ethylene-glycol salvation. The relative percentages of the four main clay mineral groups were estimated by calculating the integrated peak areas of characteristic basal reflections using Topas 2P software with the empirical factors by Biscaye (1965). Relative proportions of kaolinite and chlorite were determined from the ratio of 3.57 Å/3.54 Å peak areas. The accuracy of this method is ±5–10% for the four clay mineral groups. The illite chemistry index was calculated based on the ratio of the illite peak areas of 5 Å and 10 Å in glycol-saturated samples (Esquevin, 1969), while illite crystallinity was estimated with the full width at half maximum of the illite 10 Å peak (Ehrmann, 1998).

Strontium (Sr) and neodymium (Nd) isotopic compositions of the sediment samples in both cores were measured using a Nu Plasma HR-MC-ICP-MS instrument at the State Key Laboratory of Ore Deposit Geochemistry, Institute of Geochemistry, CAS. Because marine carbonate may contain abundant seawater Sr and thus greatly affect the $^{87}Sr/^{86}Sr$ ratio of the whole sediment sample, the organic materials and carbonate were removed from the samples by H_2O_2 and CH_3COOH, respectively. Approximately 50–100 mg of powdered sample was placed in a stainless-lined PTFE bomb, and 1 ml HF and 1 ml HNO_3 were added. The sealed bombs were then placed in an electric oven and heated to 185 °C for approximately 36 h. After cooling, the bombs were heated on a hot plate to evaporate to dryness. Then, 0.5 ml HCl was added and evaporated to dryness, and subsequently, 4 ml 1.5 mol/L HCl was added. The bomb was again sealed and placed in an electric oven at 135 °C for approximately 5 h to dissolve the residue. The resulting solution was centrifuged at 3000 rpm for approximately 3 min, and then the supernatant was loaded onto the preconditioned AG 50 W− × 8 cation exchange resin columns (8 × 100 mm) for separation of the sample matrix and Rb from Sr using 1.5 mol/L HCl. Light REEs were eluted by 6 ml 6 mol/L HCl. The solution was evaporated to dryness and dissolved with 1 ml 0.15 mol/L HCl. The solution was loaded onto the preconditioned Ln resin columns for separation of Nd from Sm. Replicate analyses of NIST SRM-987 during the study gave a mean $^{87}Sr/^{86}Sr$ of 0.710310 ± 0.000003 (2σ), close to its certified value of 0.710245. Similarly, replicate analyses of JNDi-1 gave a mean $^{143}Nd/^{144}Nd$ of 0.512112 ± 0.000004 (2σ), and its certified value is 0.511860. For convenience, the Nd isotopic ratio results are expressed as $\varepsilon_{Nd}(0) = [(^{143}Nd/^{144}Nd)_{meas}/0.512638-1]*10000$, using the present CHUR value from (Jacobsen and Wasserburg, 1980).

Planktonic foraminifera from six horizons in core YDY09 and five horizons in core 12I712 were selected for accelerator mass spectrometry (AMS) ^{14}C dating at Beta Analytic Inc. More than 20 mg of intact mixed planktonic foraminifera shells were selected from the >150 μm fractions of each sample (10 g dried sample). AMS ^{14}C-dating was used to establish the chronostratigraphic framework for both cores. All radiocarbon ages were converted and reported as calendar years before present (ka) with the Calib7.1 software program with the Marine13 calibration dataset (Reimer et al., 2013) without adjusting for a regional ^{14}C reservoir age (ΔR, deviation from the average global reservoir age of approximately 400 years, Table 1). A continuous depth-age model was performed using the Bacon software (Fig. 2), which divided a sedimentary sequence into many thin segments and estimated a linear accumulation rate for each segment based on the calibrated ^{14}C dates and a Bayesian approach (Blaauw and Christen, 2011).

To sort the grain-size distributions into geologically meaningful

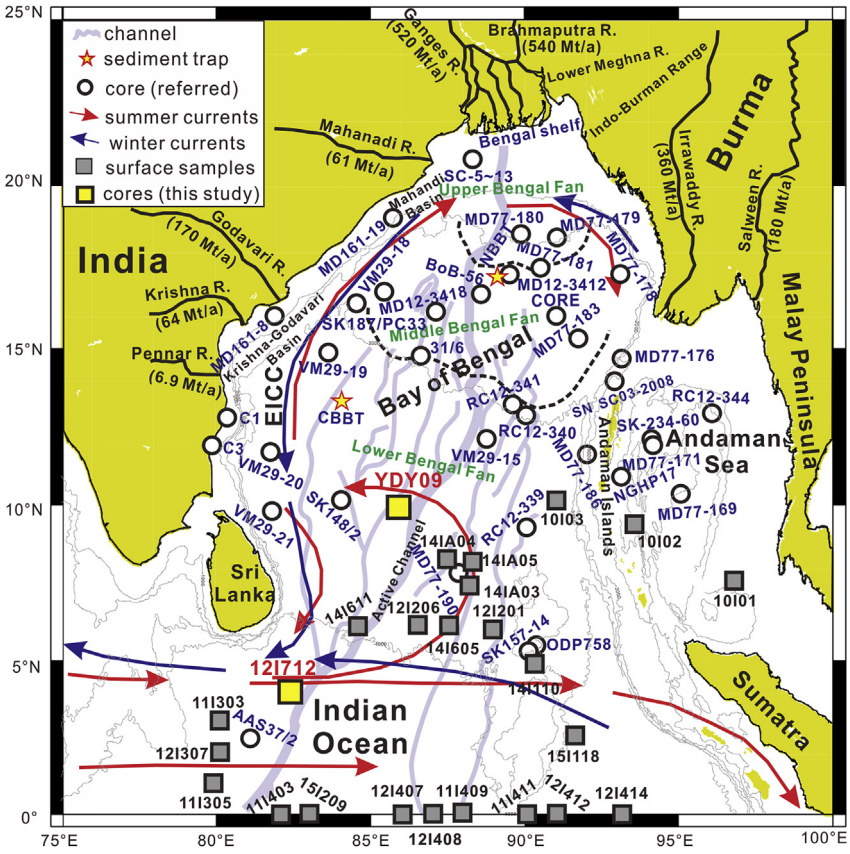

Fig. 1. Locations of gravity cores YDY09 and 12I712 (yellow squares), surface sediment samples (gray squares, this study) and the clay mineral assemblage of the sediment samples from the northeastern Indian Ocean and surrounding potential sediment source areas. Surface monsoon currents in summer (red lines) and winter (blue lines) (Schott and McCreary, 2001; Shankar et al., 2002), sediment loadings of large rivers (Milliman and Farnsworth, 2011), and the Bengal Fan and channels (gray lines, including Active Channel) are also shown (Curray et al., 2003). EICC denotes the East India Coastal Current. (For interpretation of the references to colour in this figure legend, the reader is referred to the Web version of this article.)

end-members, end-member analysis (EMA) was applied to estimate end-member variations according to the methods by Prins et al. (2000). In this study, we used algorithms for end-member modeling of compositional data (Paterson and Heslop, 2015) to determine the grain-size distributions of the detrital fraction in these two sediment cores.

3. Results

The age models are based on 11 radiocarbon dates of two cores drilled from the northeastern Indian Ocean (Table 1 and Fig. 2). Age control for the lower depth intervals from 200 cm to 266 cm of core 12I712 and from 169 cm to 244 cm of core YDY09 were obtained by linear extrapolation, assuming a constant sedimentation rate below the corresponding layers. Based on the above age model, core 12I712 covers a continuous sedimentary succession of the last ~53,000 years, whereas core YDY09 covers the last ~76,000 years. Here, we just discuss the sedimentary records of both cores over the past 50 ka.

In the Bengal Basin, sedimentation rates varied from ~11 cm/ka at core MD77-180 in the upper part (Colin et al., 1999) to ~14 cm/ka at core 31/6 in the middle part (Chauhan and Vogelsang, 2006) to

Table 1
AMS^{14}C and calibrated calendar ages and calculated sedimentation rate in cores YDY09 and 12I712 in the northeastern Indian Ocean.

Lab-ID	Depth (cm)	Materials	δ^{13}C (‰)	^{14}C ages (a BP)	Calendar ages (a BP)
391114	YDY09 3–4 cm	Mixed planktonic foraminifera	1.4	2100 ± 30	1669 ± 52
391115	YDY09 19–20 cm	Mixed planktonic foraminifera	0.8	7260 ± 30	7716 ± 42
391116	YDY09 30–32 cm	Mixed planktonic foraminifera	0.6	9490 ± 30	10323 ± 59
391117	YDY09 62–63 cm	Mixed planktonic foraminifera	0.7	13480 ± 40	15688 ± 98
408431	YDY09 124–125 cm	Mixed planktonic foraminifera	1.3	23290 ± 80	27255 ± 105
408432	YDY09 168–169 cm	Mixed planktonic foraminifera	0.9	42790 ± 600	45651 ± 534
408433	12I712 21–22 cm	Mixed planktonic foraminifera	1.3	5780 ± 30	6215 ± 36
408434	12I712 36–37 cm	Mixed planktonic foraminifera	0.8	10310 ± 30	11281 ± 56
408435	12I712 77–78 cm	Mixed planktonic foraminifera	1.1	23640 ± 90	27500 ± 94
408436	12I712 147–148 cm	Mixed planktonic foraminifera	0.7	31160 ± 160	34689 ± 164
408437	12I712 199–200 cm	Mixed planktonic foraminifera	1.3	38680 ± 370	42397 ± 251

All raw radiocarbon dates were converted to 2σ calendar ages with the CALIB 7.1.0 software using the MARINE13.14C calibration dataset (Reimer et al., 2013) without further adjustment for a regional 14C reservoir age (ΔR, deviation from the average global reservoir age of approximately 400 years).
Numbers after ± are the corresponding errors (2σ error) for the ages.

Table 2
Clay mineral compositions in sediments of the two study cores and reference cores.

No.	Numbers	Smectite	Illite	Kaolinite	Chlorite	Reference
YDY09	179	32	53	6	8	This study
12I712	249	38	48	6	7	This study
Ganges R.	30	29	56	6	9	Hafijur et al., (unpublished)
Brahmaputra R.	33	1	78	10	11	Hafijur et al., (unpublished)
Meghna R.	62	3	66	12	19	Hafijur et al., (unpublished)
GBM	7	8	66	8	17	Hafijur et al., (unpublished)
Mahanadi R.	9	18	54	23	5	Bejugam and Nayak (2016a)
Irrawaddy R.	48	60	15	20	5	Rodolfo (1969)
Godavari R.	9	49	22	25	5	Bejugam and Nayak (2016a)
Krishna R.	9	66	13	17	3	Bejugam and Nayak (2016a)
Pennar R.	5	51	31	14	4	Bejugam and Nayak (2016a)
Sumatra	14	9	16	67	7	Liu et al. (2012)
Malaysia	12	0	30	69	1	Liu et al. (2012)
Bengal shelf	67	24	50	21	4	Segall and Kuehl (1992)
SC-10	NA	10	71	16	3	Bejugam and Nayak (2016b)
SC-05	NA	12	70	13	5	Bejugam and Nayak (2016b)
SC-06	NA	9	73	12	5	Bejugam and Nayak (2016b)
SC-11	NA	16	67	13	4	Bejugam and Nayak (2016b)
SC-09	NA	14	69	14	3	Bejugam and Nayak (2016b)
SC-12	NA	18	65	14	4	Bejugam and Nayak (2016b)
SC-13	NA	14	69	15	2	Bejugam and Nayak (2016b)
MD161-19	28	38	37	19	6	Mazumdar et al. (2015)
MD77-179	NA	53	23	8	17	Colin et al. (1999)
MD77-181	NA	48	24	10	18	Colin et al. (1999)
MD77-178	NA	56	16	8	19	Colin et al. (1999)
MD12-3412	14	14	56	7	22	Joussain et al. (2016)
NBBT-D[b]	13	27	52	12	10	Ramaswamy et al. (1997)
BoB-56	151	3	66	12	19	Li et al. (2018)
MD12-3418	11	16	62	4	17	Joussain et al. (2017)
CORE?[a]	14	24	56	6	13	Reddy and Rao, 2001
KL31/1	21	19	25	25	32	Chauhan et al. (2004)
MD161-8	45	62	15	18	6	Mazumdar et al. (2015)
MD77-183	NA	59	16	9	16	Colin et al. (1999)
31/6	13	25	54	9	13	Chauhan and Vogelsang (2006)
MD77-176	NA	62	14	9	15	Colin et al. (1999)
SN SC03-2008	21	38	33	16	13	Nagasundaram et al. (2014)
CBBT-D[b]	13	39	36	14	11	Ramaswamy et al. (1997)
RC12-341	NA	54	20	9	17	Colin et al. (1999)
RC12-340	NA	45	25	9	21	Colin et al. (1999)
C1	6	70	11	16	3	Symphonia and Nathan (2018)
C3	7	33	14	49	4	Symphonia and Nathan (2018)
MD77-186	NA	86	7	4	4	Colin et al. (1999)
SK148/2	25	8	60	14	18	Kessarkar et al. (2005)

NA: no data available. All data are (re)calculated according to Biscaye (1965).
[a] Without core name in the paper.
[b] CBBT-D and NBBT-D denote the deep sediment traps at the corresponding sites.

~8 cm/ka at core SK148/2 in the lower part of the basin (Kessarkar et al., 2005), and around the Ninetyeast Ridge, the sedimentation rates are ~3–5 cm/ka at cores SK157-14, SK157-15 and SK157-16 (Ahmad et al., 2005; Raza et al., 2014) or even approximately 2 cm/ka at core Ocean Drilling Program (ODP) Site 758 (Gourlan et al., 2010), although sedimentation rates at core MD12-3418 in the middle part of the basin reached an average of 0.1 cm/yr due to turbidite activity (Joussain et al., 2017). At core 12I712 outside the BoB, linear sedimentation rates fluctuated between 2 cm/ka and 6 cm/ka with an average value of 4.73 cm/ka, while at core YDY09 inside the BoB, sedimentation rates ranged between 2 cm/ka and 10 cm/ka with an average of 4.35 cm/ka (Fig. 2). Thus, the lower sedimentation rates (4–5 cm/ka) in the two study cores were in accordance with the normal sedimentation rate in the region and were less connected to turbidite activity in the Bengal Fan (Joussain et al., 2016; Fournier et al., 2017), which was correlated with its distance from the sediment input of the surrounding land and the Active Channel.

Core sediments in the study area consist predominantly of silt and clay, while sand was only a minor component (average less than 5%, Fig. 2). At core YDY09 in the north, sediments were slightly finer grained, and the silt percentages varied between 47% and 76%, with an average of 60%, while the clay percentages ranged from 20% to 49%, with an average of 37%. By contrast, at core 12I712 in the south, the silt percentages varied between 45% and 84%, with an average of 69%, while the clay percentages ranged from 7% to 55%, with an average of 29%.

Despite probable overestimation of the non-spherical natural particles (Konert and Vandenberghe, 1997; Garzanti et al., 2011), today, laser granulometry data are widely utilized to reflect hydrodynamical conditions in different depositional environments (e.g., Hao et al., 2012; Huang et al., 2018; Jin et al., 2019), and here we also insist on laser grain-size measurement considering the well-repeated data when we measured the samples using the laser method. To identify the number of grain-size end-members (EM) that were mixed within the sediment, further reveal the grain-size distributions of different end-members and to quantify the proportion of each end-member over time (Paterson and Heslop, 2015), EMA was applied to the 244 and 77 grain-size samples analyzed for the detrital fraction of cores 12I712 and YDY09, respectively. The goodness of fit statistics show that the three end-member model is the best optimization between the number of

Table 3
$^{87}Sr/^{86}Sr$ and ε_{Nd} in sediments of the two study cores and reference cores.

Sample	Numbers	$^{87}Sr/^{86}Sr$	ε_{Nd}	References
YDY09	20	0.723	−11.90	This study
12I712	20	0.732	−14.05	This study
Ganges R.	21	0.775	−18.01	Lupker et al. (2013)
Brahmaputra R.	13	0.736	−16.24	Lupker et al. (2013)
Lower Meghna R.	9	0.737	−15.79	Lupker et al. (2013)
Godavari R.	3	0.725	−16.38	Ahmad et al. (2009)
Krishna R.	3	0.724	−12.38	Ahmad et al. (2009)
Pennar R.	2	0.757	−22.70	Ahmad et al. (2009)
Barren Island (Andaman Sea)	12	0.704	5.57	Chandrasekharam et al. (2009)
Irrawaddy R.	NA	0.713	−10.67	Colin et al. (1999)
Indo-Burman Range	10	0.713	−4.86	Licht et al. (2013)
Deccan Traps	NA	0.710	−5.00	Tripathy et al. (2011)
MD77-180	23	0.724	−11.71	Joussain et al. (2016)
MD77-179	NA	0.720	−12.82	Colin et al. (1999)
MD77-181	NA	0.720	−12.48	Colin et al. (1999)
MD77-178	NA	0.715	−8.56	Colin et al. (1999)
MD12-3412	47	0.725	−10.86	Joussain et al. (2016)
VM29-18	NA	0.724	−15.06	Colin et al. (1999)
SK187/PC33	36	0.739	−15.57	Tripathy et al. (2011)
MD77-183	NA	0.715	−9.03	Colin et al. (1999)
VM29-19	NA	0.723	−13.93	Colin et al. (1999)
MD77-176	11	0.716	−8.73	Colin et al. (2006)
RC12-341	NA	0.714	−10.28	Colin et al. (1999)
RC12-344	NA	0.717	−11.29	Colin et al. (1999)
RC12-340	NA	0.716	−10.40	Colin et al. (1999)
VM29-15	NA	0.712	−10.79	Colin et al. (1999)
SK-234-60	31	0.711	−7.39	Awasthi et al. (2014)
MD77-171	NA	0.712	−9.25	Colin et al. (1999)
VM29-20	NA	0.726	−16.13	Colin et al. (1999)
MD77-186	NA	0.715	−10.87	Colin et al. (1999)
MD77-169	45	0.717	−10.51	Colin et al. (2006)
SK148/2	11	0.731	−18.70	Kessarkar et al. (2005)
VM29-21	NA	0.732	−16.17	Colin et al. (1999)
RC12-339	NA	0.714	−11.51	Colin et al. (1999)
MD77-190	NA	0.714	−10.73	Colin et al. (1999)
ODP Site 758	6	0.723	−12.14	Gourlan et al. (2010)
SK-157-14	28	0.715	−13.75	Ahmad et al. (2005)
AAS37/2	8	0.725	−14.39	Kessarkar et al. (2005)

NA: no data available.

subpopulations and r^2 (>90% of the variance). At core 12I712, the three end-member model contains grain-size modes of ~2, ~5, and ~13 μm for end-members EM1, EM2, and EM3, respectively (Fig. 3c). The proportion of EM1 varies between ~20% and 100% (average of ~60%), with the highest values from 37 to 31 ka and low values during the stages of 50–45 ka, 42–37 ka and 31–28.5 ka (Fig. 4). The proportion of EM2 (which varies from 0% to ~60%, average of 30%) shows a simultaneous change in the illite percentage, which reaches the peaks during the high illite percentage stages of 50–45, 42–37 and 31–28.5 ka. The proportion of EM3 (which varies between 0% and 60%, average of 10%) shows great variations since the last glacial maximum (LGM) compared with the former stages. By contrast, at core YDY09, the three end-member model contains grain-size modes of ~3, ~8, and ~41 μm for end-members EM1, EM2, and EM3, respectively (Fig. 3f). The proportion of EM1 varies between ~15% and ~70% (average of 45%), with higher values before the LGM (Fig. 4). The proportion of EM2 (which varies from ~10% to ~65%, average of 40%) simultaneously shows a high illite percentage, which reaches peaks from 24 to 20 ka and from 14 to 9 ka. The proportion of EM3 (which varies between 0% and 30%, average of 15%) shows low values after the LGM.

As the dominant clay mineral in both cores, illite, which mainly originates from the G-B Rivers, ranges from 21% to 87% of the clay component in core YDY09, with an average value of 52%, but varies from 6% to 79% of the clay component in core 12I712, with an average value of 50% (Fig. 5). As the second major clay mineral in the study area, smectite, which is related to the alteration of volcanic materials from eastern India, ranges between 6% and 88% in core 12I712, with an average of 37%, but ranges between 3% and 71% in core YDY09, with an average of 33%. As minor clay minerals, both kaolinite, which is sourced from the Malay Peninsula and Sumatra Islands, and chlorite, which is a characteristic mineral of the Ganges River, have a 6–9% average composition in the core sediments. According to the clay mineral assemblage of the abovementioned potential sources, the sediments in the two cores 12I712 and YDY09 were likely a mixture of sediments derived from the G-B Rivers and eastern Indian rivers (Fig. 6).

In core YDY09, the $^{87}Sr/^{86}Sr$ ratios range from 0.716070 to 0.741681 with an average of 0.722758, while ε_{Nd} values range from −14.74 to −10.30, with an average of −11.90; by contrast, in core 12I712, the $^{87}Sr/^{86}Sr$ ratios range from 0.722147 to 0.741790, with an average of 0.732013, while ε_{Nd} values range from −16.61 to −12.12 with an average of −14.05 (Fig. 7). At core YDY09, both Sr and Nd isotopes show a significant change at ~26 ka, when $^{87}Sr/^{86}Sr$ ratios increased rapidly from 0.717 to 0.734, while ε_{Nd} values decreased abruptly from −10.48 to −14.00, especially during 24–19 ka (GB2) and 14–9 ka (GB1) when $^{87}Sr/^{86}Sr$ ratios reached a peak (Fig. 8). This finding probably indicates the strengthened sediment supply from the G-B Rivers during these stages. However, at core 12I712, $^{87}Sr/^{86}Sr$ ratios during the three stages of 50–45 ka (GB5), 42–37 ka (GB4) and 31–28.5 ka (GB3) were clearly higher than those during other stages, confirming that sediments during these stages were more derived from the G-B Rivers to the north.

Sedimentary records at both cores changed abruptly just before

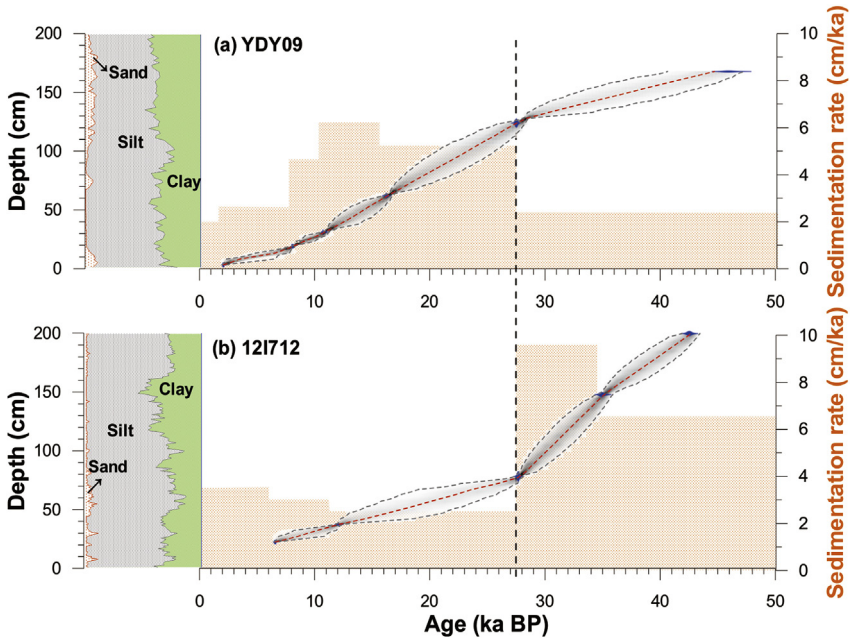

Fig. 2. Age-depth relationship and calculated sedimentation rates (orange shadows) of cores YDY09 and 12I712. The age-depth relationship was calculated with a Bayesian approach using the Bacon software overlying the distributions of the individual dates (blue). The line curve shows the best model (red line: mean), and the area between the blue lines indicates chronological uncertainties (the model's 95% probability interval). The dashed lines represent abrupt changes in the sedimentation rate in the study area. On the left, we also show the grain-size compositions of the core sediments in the study area. (For interpretation of the references to colour in this figure legend, the reader is referred to the Web version of this article.)

the LGM. The sedimentation rate at core YDY09 increased greatly from ~2 cm/ka to ~6 cm/ka at approximately 28 ka, when the sedimentation rate at core 12I712 decreased sharply from ~10 cm/ka to less than 3 cm/ka. Due to limited measured dates for both cores, we can deduce that this time of ~28 ka is in accordance with the abrupt change in clay minerals and grain size at ~26 ka. During this time, the sand content at core YDY09 increased, while the sand content at core 12I712 decreased (Fig. 2). The sorting coefficient at core YDY09 decreased quickly just before the LGM, while sediments at core 12I712 became coarse grained with the result of decreasing mean grain size (unit: Φ, Fig. 4). The smectite percentage at core YDY09 remained high before the LGM, when the illite percentage was low in the core sediments. By contrast, at core 12I712, the smectite percentage has remained high since the LGM, when the illite percentage was stably low (Fig. 5).

At the same time, both grain-size parameters and clay mineral compositions show staged changes in the study area. Normally, the smectite percentage in the two study cores was high, while the illite percentage was low (Fig. 6), which was correlated with sediment supply by the surrounding potential sources (Indian rivers and the Irrawaddy River) and weathering of volcanic materials that were characterized by a high smectite percentage (Rodolfo, 1969; Venkatar and Biscaye, 1973; Phillips et al., 2014; Bejugam and Nayak, 2016a). However, there are five stages with low smectite percentages but high illite percentages in the core sediments: 50–45 ka, 42–37 ka, 31–28.5 ka, 24–20 ka and 14–9 ka. Since the G-B river system has a high illite percentage (averaging 66%) and a low smectite percentage (averaging 8%) in its sediments, we can suggest that sediment supply by the Himalayas to the north peaked during the above five stages (Fig. 4).

During the LGM, sediments in core YDY09 became less sorted than before, while sediments in core 12I712 became coarse-grained (Fig. 4), indicating that hydrodynamical conditions were strong and more fluvial particles could be loaded into the two study cores. The smectite percentage decreased greatly, while the illite percentage increased until the peak at core YDY09 (Fig. 5), confirming that more sediments of the Himalayas were transported through the G-B river system into the study area under the impact of monsoon climate change and sea-level fluctuation (Li et al., 2018; Weber and Reilly, 2018).

4. Discussion

4.1. Sediment provenance

There are distinct clay mineral assemblages for the potential surrounding sediment sources of the northeastern Indian Ocean. To the north, the G-B river system (Datta and Subramanian, 1997) and Mahanadi River (Bejugam and Nayak, 2016a) have a high illite percentage in the sediments (Fig. 6) because illite is mainly a product of glacial weathering under arid conditions, with its source being the Himalayan region (Bejugam and Nayak, 2016b). To the northwest, sediments from eastern India via the Godavari, Krishna and Pennar Rivers are characterized by a high smectite percentage (Raman et al., 1995; Bejugam and Nayak, 2016a), resulting in a high smectite percentage in the sediments of the Krishna-Godavari Basin and neighboring sea areas (Raman et al., 1995; Chauhan and Vogelsang, 2006). To the northeast, sediments from the Irrawaddy River are also characterized by a high smectite percentage, and they are mostly deposited in the Andaman Sea, resulting in a high smectite percentage in the neighboring sea area of the river mouth (Awasthi et al., 2014; Ali et al., 2015); additionally, some of the sediments were transported westward towards the BoB during the NE monsoon (Ramaswamy et al., 2004; Rao et al., 2005). To the east, the sediments of Malay Peninsula and Sumatra have the highest kaolinite percentage (Liu et al., 2012), which is clearly distinguished from that of the study area but hardly affects the depositional environments in the study area according to distinct clay mineral assemblages in these sediments, as shown in Fig. 6. This finding is confirmed by the existence of the Ninetyeast Ridge,

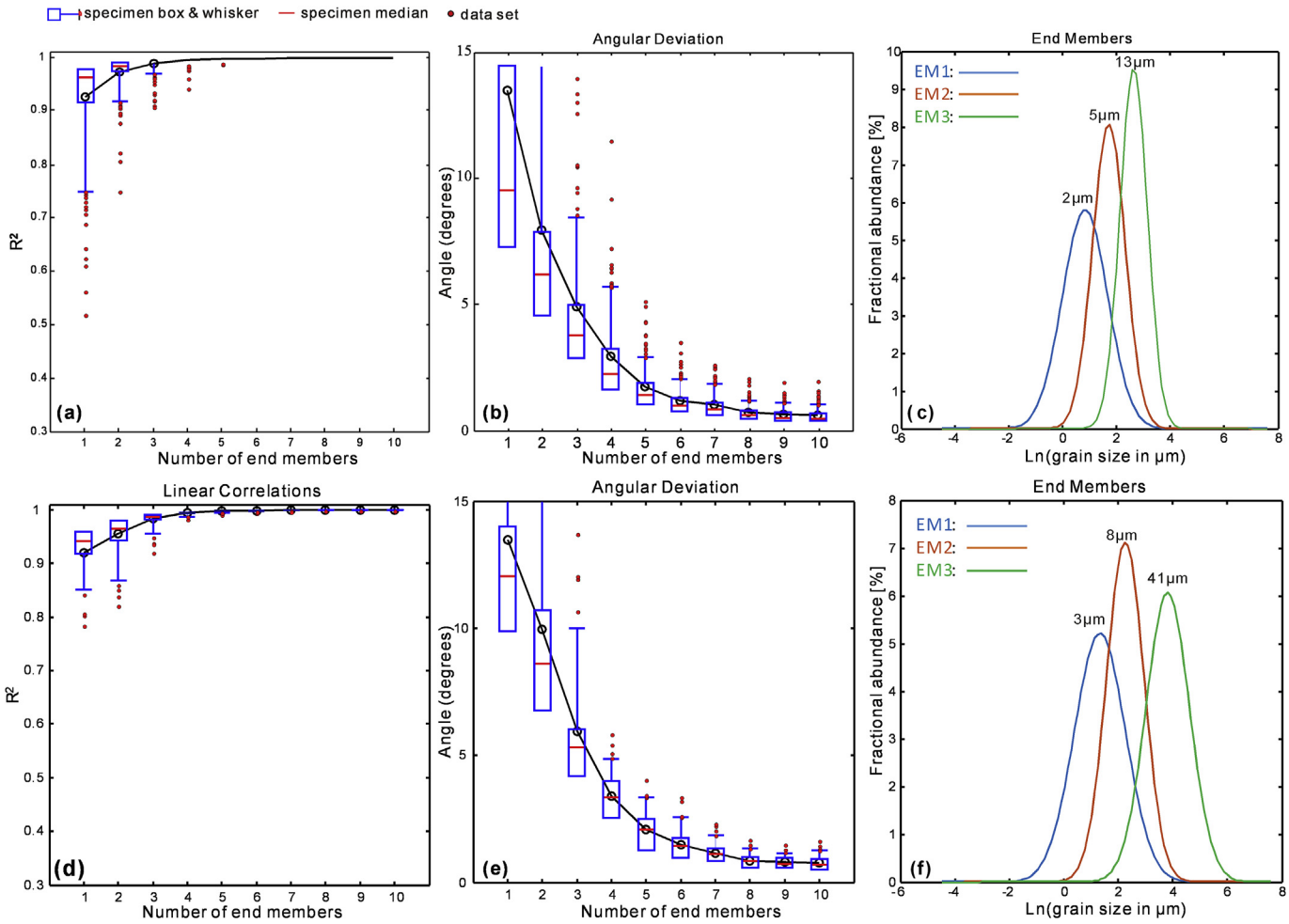

Fig. 3. End-member modeling results of the terrigenous fraction in the sediments of cores 12I712 and YDY09. Coefficients of determination (r^2) for each model size class with 1–10 end-members in (a) cores 12I712 and (d) YDY09 and angular differences (in degrees) between the reconstructed and observed data sets as a function of the number of end-members. The goodness of fit statistics demonstrate that the three end-member model provides the best compromise between the number of end-members and r^2 (more than 90% of the variance) in (b) cores 12I712 and (e) YDY09, and three end-members of the terrigenous fraction of sediments in (c) cores 12I712 and (f) YDY09 were modeled. Grain-size modes for end-members EM1, EM2, and EM3 are ~2, ~5, and ~13 μm for core 12I712 and ~3, ~8, and ~41 μm for core YDY09, respectively.

where the deep waters in the BoB originate in the circumpolar region and flow northward (Warren, 1981), which prevents more sediments in Sumatra and Malay Peninsula from being transported westward into deep-sea environments of the northeastern Indian Ocean. Therefore, sediments in the eastern and central regions of the middle Bengal Fan are mostly of Himalayan source, while the western part is predominantly from the Indian Peninsula (Chauhan and Vogelsang, 2006). Considering the clay mineral distribution in surface sediment samples from the northeastern Indian Ocean (Fig. 6), combined with much higher sediment input from the Irrawaddy River than from rivers in the eastern Indian Peninsula and the close distance to the Irrawaddy River mouth and Indo-Burman Ridge, we assume that both the G-B Rivers (mainly through the widely developed channels) and the Myanmar source provide most of the particles in the eastern Bengal Fan. Evidence from sediment trap experiments further revealed that modern terrigenous flux into the BoB was dominantly derived from the G-B Rivers (Ramaswamy et al., 1997; Unger et al., 2003).

Recent Integrated Ocean Drilling Program (IODP) expeditions revealed that the Bengal Fan is a sand-rich turbiditic system (Weber and Reilly, 2018; Weber et al., 2018). The clay dispersal patterns may be different from the sand dispersal patterns, and provenance inferences based on clay mineral data can hardly be extrapolated to sand and hence to the whole sediment system. To better explain the fine-grained sediment sources of the two cores, we further measured Nd and Sr isotopes of both cores in the study area. Nd and Sr isotope signatures can provide information on sediment sources in the BoB (Colin et al., 1999; Tripathy et al., 2011; Awasthi et al., 2014; Joussain et al., 2016), and here, we similarly use them for additional constraints. The ε_{Nd} values and $^{87}Sr/^{86}Sr$ ratios of cores YDY09 (average $\varepsilon_{Nd} = -11.90$, $^{87}Sr/^{86}Sr = 0.723$) and 12I712 (average $\varepsilon_{Nd} = -14.05$, $^{87}Sr/^{86}Sr = 0.732$) are significantly more radiogenic than the published data for the Ganges River (average $\varepsilon_{Nd} = -18.01$, $^{87}Sr/^{86}Sr = 0.775$), Brahmaputra River (average $\varepsilon_{Nd} = -16.24$, $^{87}Sr/^{86}Sr = 0.736$) and lower Meghna River (average $\varepsilon_{Nd} = -15.79$, $^{87}Sr/^{86}Sr = 0.737$ (Lupker et al., 2013),) to the north, less radiogenic than those for the Deccan Traps (average $\varepsilon_{Nd} = -5.00$, $^{87}Sr/^{86}Sr = 0.710$ (Tripathy et al., 2011),) to the northwest and Barren Island Volcano (average $\varepsilon_{Nd} = 5.57$, $^{87}Sr/^{86}Sr = 0.704$ (Chandrasekharam et al., 2009),), Indo-Burman Range (average $\varepsilon_{Nd} = -4.86$, $^{87}Sr/^{86}Sr = 0.713$ (Licht et al., 2013),) and Irrawaddy River (average $\varepsilon_{Nd} = -10.67$, $^{87}Sr/^{86}Sr = 0.713$ (Colin et al., 1999),) to the northeast, and similar to those for the Godavari River (average $\varepsilon_{Nd} = -16.38$, $^{87}Sr/^{86}Sr = 0.725$) and Krishna River (average $\varepsilon_{Nd} = -12.38$, $^{87}Sr/^{86}Sr = 0.724$ (Ahmad et al., 2009),) to the northwest (Fig. 7). The obviously different ε_{Nd} values and

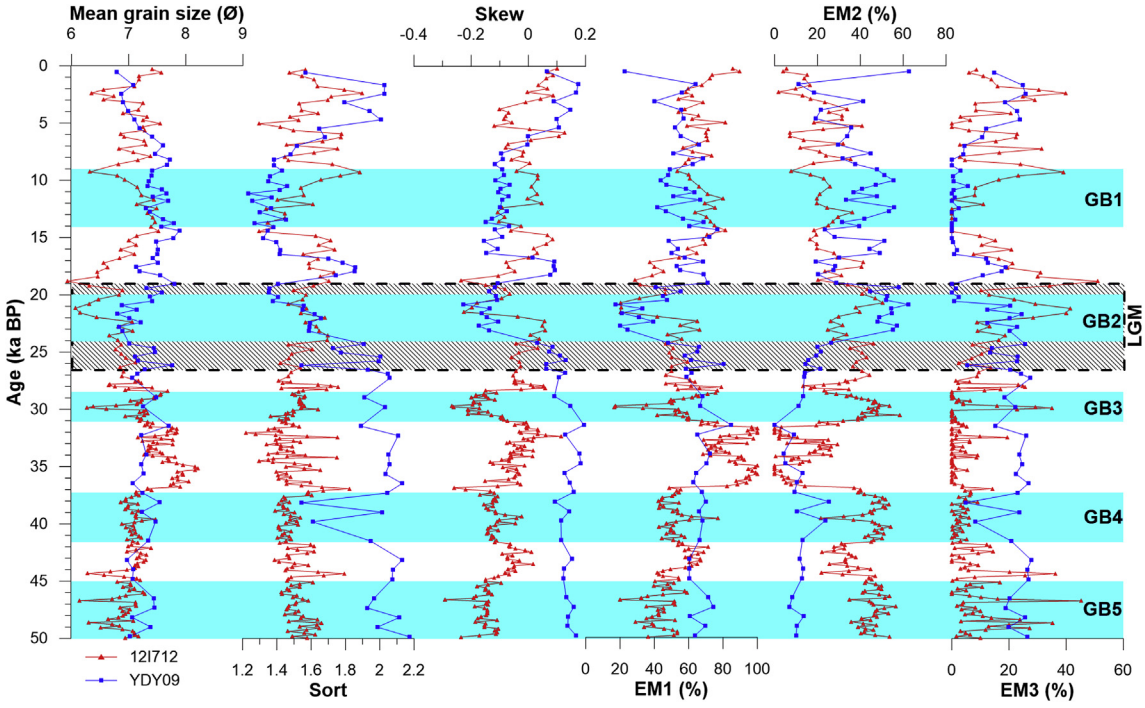

Fig. 4. Grain-size parameters (mean grain size, sort, skew and kurt) and three calculated end-members for cores 12I712 (red) and YDY09 (blue). The five shades upward represent heavy sediment supply of the G-B river system (GB1-GB5) discussed in the text, which happened at 50–45 ka, ~42–37 ka, 31–28.5 ka, 24–20 ka and 14–9 ka. The LGM, which happened between 26.5 and 19 ka (Clark et al., 2009), is marked with a dashed square filled with slashes. (For interpretation of the references to colour in this figure legend, the reader is referred to the Web version of this article.)

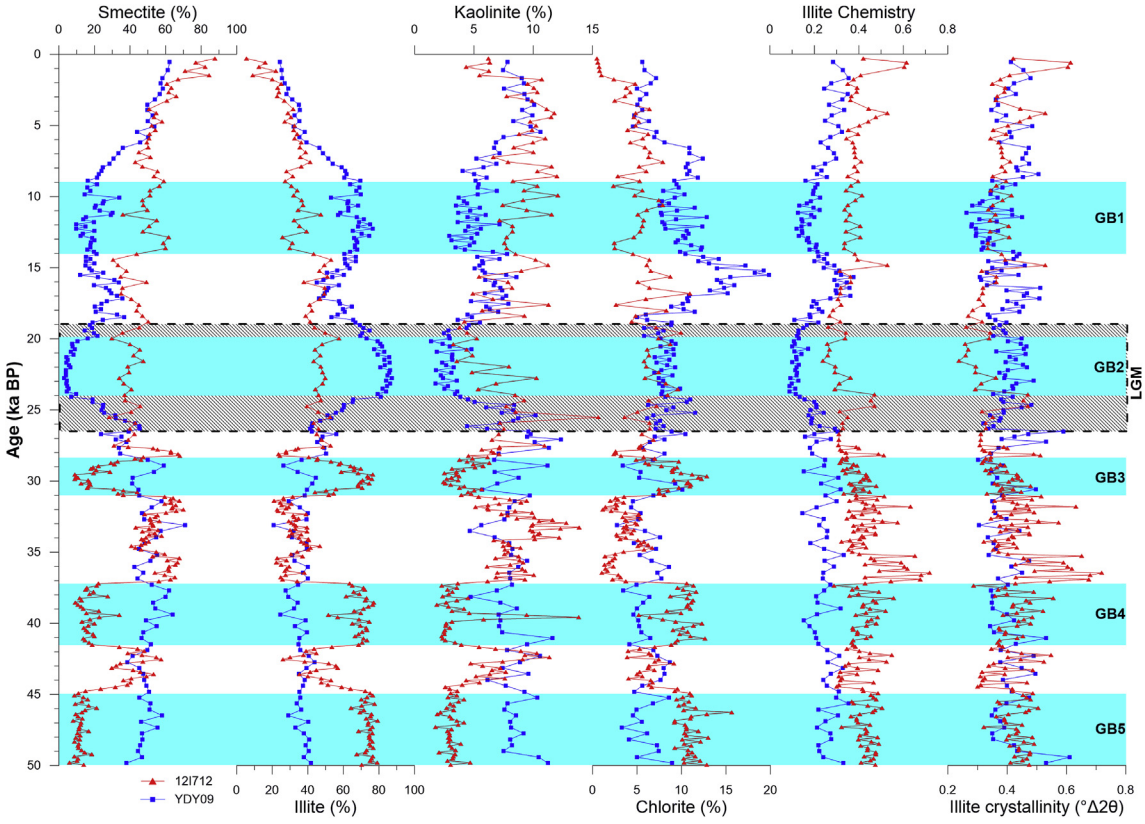

Fig. 5. Four main clay mineral percentages, illite chemistry and illite crystallinity in cores 12I712 (red) and YDY09 (blue). The five shades upward represent heavy sediment supply by the G-B river system (GB1-GB5) indicated by clay mineral differences, which happened at 50–45 ka, 42–37 ka, 31–28.5 ka, 24–20 ka and 14–9 ka. The LGM is marked with a dashed square filled with slashes. (For interpretation of the references to colour in this figure legend, the reader is referred to the Web version of this article.)

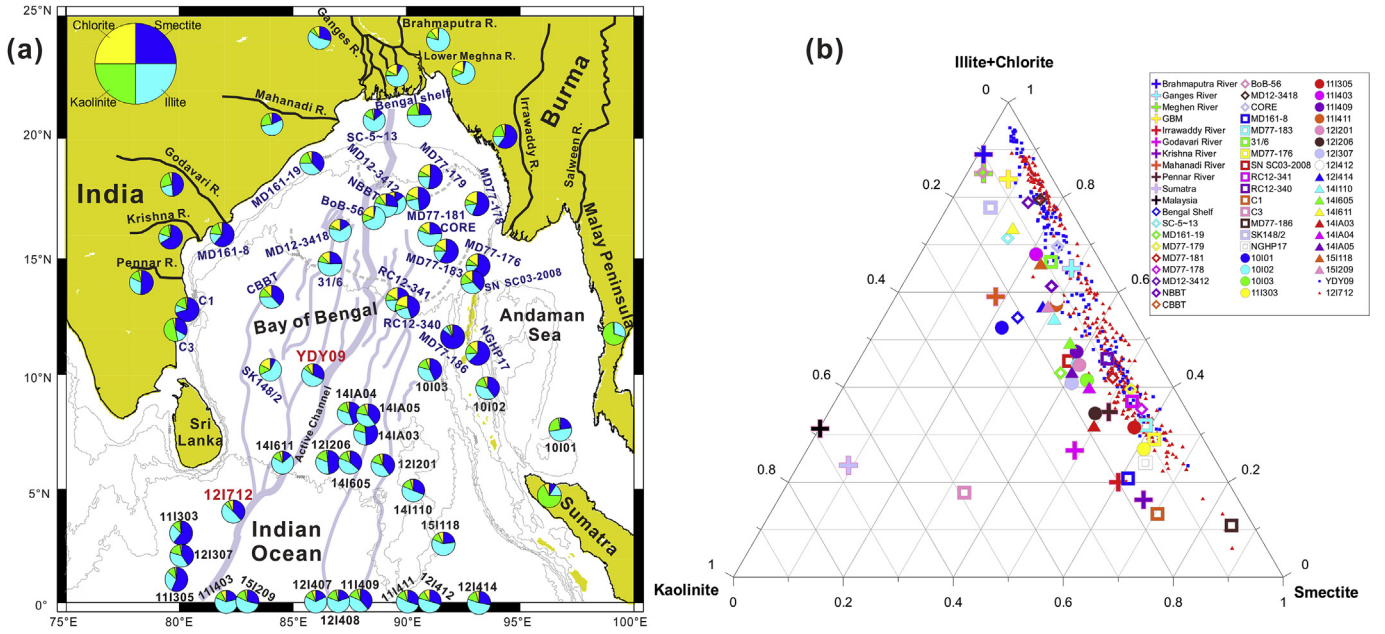

Fig. 6. (a) Distribution of clay mineral compositions and (b) ternary diagram showing the clay mineral assemblage of the above possible sources. Channels (gray lines, including Active Channel) are redrawn from Curray et al. (2003). See Table 2 for the clay mineral data of the related references.

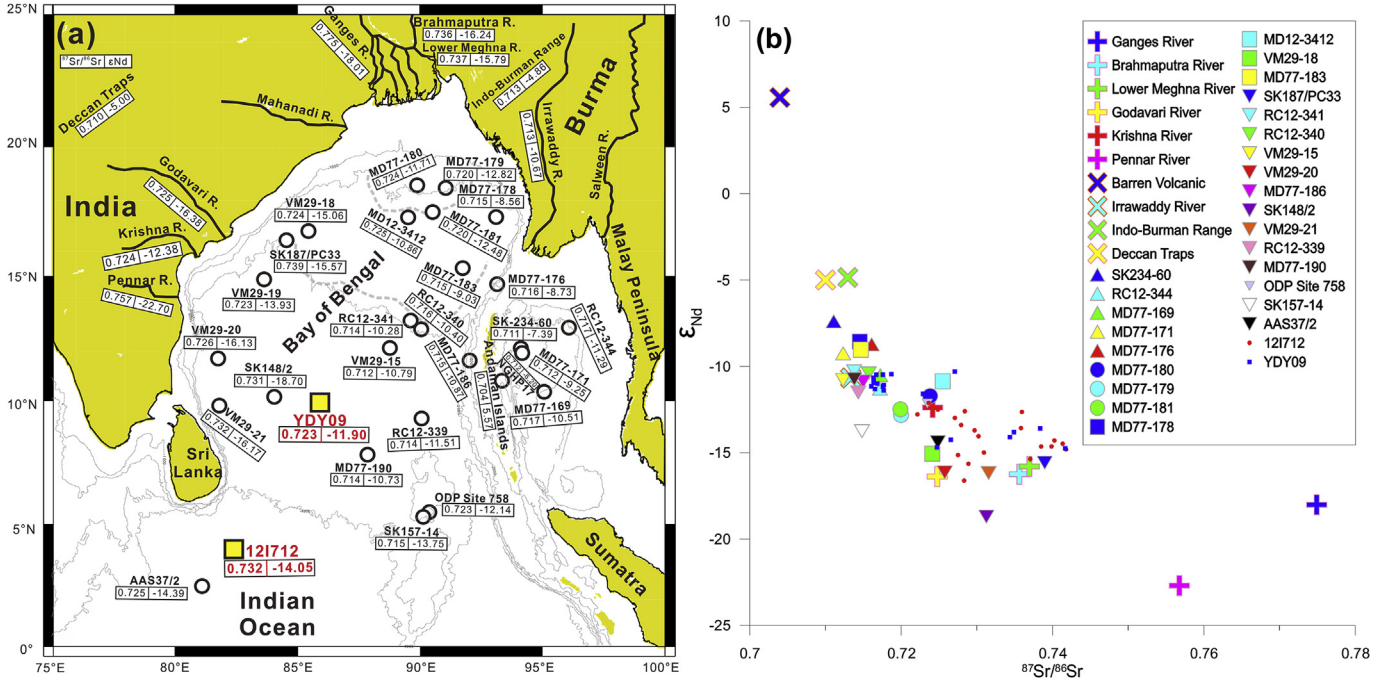

Fig. 7. (a) Distribution of the $^{87}Sr/^{86}Sr$ ratios (first numbers in the squares) and ε_{Nd} values (second numbers in the squares) and (b) discrimination diagram of ε_{Nd} vs. $^{87}Sr/^{86}Sr$ for the potential sources, referenced cores and study gravity cores in the northeastern Indian Ocean and neighboring Bay of Bengal and Andaman Sea. See Table 3 for the Sr and Nd isotope data of the related references.

$^{87}Sr/^{86}Sr$ ratios of the core sediments compared to those of Barren Island Volcano, and Pennar and Ganges Rivers suggest the very limited sediment supply from the above sources to the study area. The Pennar River has a clearly smaller sediment loading than other rivers in eastern India (Milliman and Farnsworth, 2011), while the Barren Island (belonging to the Andaman Islands) Volcano has already been shown to be limited compared with terrigenous sediment supply due to its distinguished mineralogy and chemistry (Awasthi et al., 2014). Thus, sediment supply from the Pennar River and Barren Island Volcano can be easily excluded from the significant potential sources of the study area. Meanwhile, the similar ε_{Nd} values and $^{87}Sr/^{86}Sr$ ratios of core sediments to those of the Brahmaputra and lower Meghna Rivers to the north, Godavari and Krishna Rivers and Deccan Traps to the northwest, and Indo-Burman Range to the northeast indicate the likely mixture of the above sources for the two study cores, which is in accordance with the Nd and Sr evidence that indicated that the western BoB is mainly supplied by the G-B river system, whereas the eastern BoB is

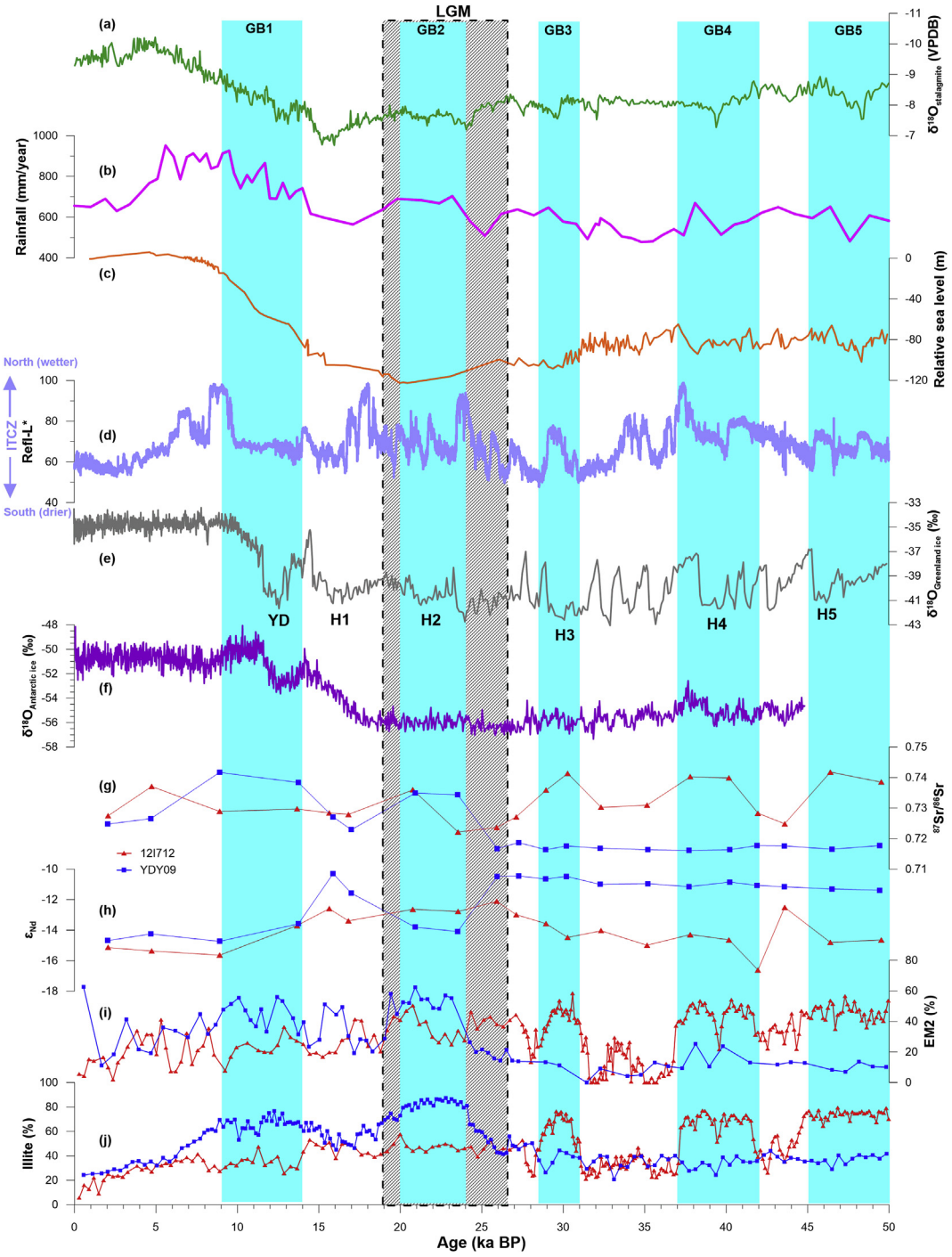

Fig. 8. Comparison of (a) monsoon evolution (cave stalagmites from Borneo (Carolin et al., 2016)), (b) rainfall variation in East Asian summer monsoon rainfall from Chinese loess (Beck et al., 2018), (c) the ITCZ shift (recorded in the Arabian Sea (DiNezio and Tierney, 2013)), (d) global sea-level fluctuation (redrawn from (Liu et al., 2017)), (e) oxygen isotopes of ice sheets in Greenland (Grootes et al., 1993), (f) oxygen isotopes of ice sheets in Antarctic (Stenni et al., 2004), (g) $^{87}Sr/^{86}Sr$ ratios, (h) ε_{Nd} values, (i) EM2 and (j) illite percentages in the two study cores YDY09 (blue) and 12I712 (red) in the eastern Indian Ocean. The five shades (GB1-GB5) leftward represent heavy sediment supply by the G-B Rivers discussed in the text, which happened at 50–45 ka, 42–37 ka, 31–28.5 ka, 24–20 ka and 14–9 ka. The LGM is marked with a dashed square filled with slashes. YD and H1–H5 denote the Younger Dryas and Heinrich events 1–5, respectively. (For interpretation of the references to colour in this figure legend, the reader is referred to the Web version of this article.)

mixed by materials from the Himalayan and Indo-Burman Ranges (Colin et al., 1999).

4.2. Sediment transport patterns

In the study area, the fine (2–3 μm, EM1) and intermediate (5–8 μm, EM2) end-members at cores YDY09 and 12I712 are mainly associated with fluvial inputs from the Indian Peninsula to the northwest and from the Himalayas to the north through the G-B river system, respectively. The highest abundances of EM1 is in accordance with the high smectite percentage (Figs. 4 and 5), indicating that EM1 was probably related to predominantly fluvial inputs from the Indian Peninsula, where the Indian river-originated sediments are characterized by a high smectite percentage

(Bejugam and Nayak, 2016a). The proportion of intermediate EM2 matches well with the illite percentage of the two cores, suggesting that this end-member might represent sediment supply by the G-B river system. The coarse end-member (EM3) of the two sediment cores might be correlated with eolian deposits in the eastern Indian Ocean, which are also coarser grained than particles of other sources (Grand et al., 2015; Gherboudj et al., 2017), well-developed turbidites in the submarine Bengal Fan (Fournier et al., 2017; Weber and Reilly, 2018) or volcanic activities in the northern Indian Ocean (Chandrasekharam et al., 2009; Ismaiel et al., 2017).

In the Andaman Sea, the SW monsoon shifted southward from the Himalayas into Myanmar and the Andamans, resulting in higher sediment contributions from rocks of the Indo-Burman-Arakan and eastern Andamans, which probably correlated with an eastward flowing surface current that brought sediments from the Bengal shelf and western margin of Myanmar into the central and southern parts of the Andaman Sea, especially since the LGM (Awasthi et al., 2014). In the western BoB, fluvial sediments of the G-B, Godavari, Krishna and Mahanadi Rivers were mainly transported southward under the EICC effect in winter (Shankar et al., 2002; Wijesekera et al., 2015; Sarma et al., 2018), especially during the LGM when the summer southwest monsoon was weak (Tiwari et al., 2005). At the same time, sediments derived from the G-B Rivers were transported to the deep ocean through the Active Channel (Kottke et al., 2003; Rogers et al., 2015; Fournier et al., 2017) that directly connected the G-B Rivers to the Bengal Fan because of its interruption of the westward along-shelf transport of riverine sediments (Segall and Kuehl, 1992, Fig. 1). Moreover, the nepheloid layer is much stronger in the western BoB, indicative of strong turbulence and a high concentration of suspended sediment from the Indian rivers that has abundant smectite (Kolla et al., 1976). Therefore, the whole submarine Bengal Fan and neighboring areas were intensively impacted by sediments from large rivers to the north (Ramaswamy et al., 1997; Unger et al., 2003; Nagasundaram et al., 2014; Phillips et al., 2014), especially in the western BoB, which was mainly affected by sediments from eastern India (Chauhan and Vogelsang, 2006). In the study area, the essential force transporting the river-sourced sediments is the northeast surface currents in winter that flow from the west and the north. Other important passageways are widely developed channels that load sediments of the G-B Rivers into the Bengal Fan (Fig. 1).

4.3. Climatic impact

Despite the substantial transformation of the depositional environment at 26 ka, there were also five significant stages (GB1~GB5) with high $^{87}Sr/^{86}Sr$ ratios, low ε_{Nd} values, high EM2 percentages and high illite percentages in the study area that occurred at 50–45 ka, 42–37 ka, 31–28.5 ka, 24–20 ka and 14–9 ka (Fig. 8). During these periods, sediment supply by the G-B river system reached the maximum.

The time of staged sediment supply from the G-B river system that coincided with sediment source changes at core Sk-234-60 in the Andaman Sea (Awasthi et al., 2014) has been simultaneous with global cold climate events (Younger Dryas and Heinrich events) over the past 50 ka, in addition to matching well with monsoon records from stalagmite and Chinese loess (Fig. 8). During cold episodes, variations in the boundary conditions at high latitudes can modify the cold air transported towards the south (Zonneveld et al., 1997); consequently, the SW monsoon is weakened, and the NE monsoon is strengthened (Ahmad et al., 2005). Heavy sediment supply from the G-B river system happens when the monsoon weakens, rainfall increases and the climate in polar ice sheets becomes cold. During these stages, more sediment transfer of the G-B river system caused by monsoon rainfall changes (Joussain et al., 2017) was discharged into the BoB and contributed to the fast accumulation of sediments in the submarine Bengal Fan (Joussain et al., 2016). Previous studies also revealed that there have been higher sediment contributions to both the BoB and neighboring Andaman Sea since the LGM due to increasing monsoonal precipitation and resultant enhanced chemical weathering in the Himalayan system and Indian Peninsula (Tripathy et al., 2011; Lupker et al., 2013; Awasthi et al., 2014). In the Andaman Sea, low smectite percentages and high $^{87}Sr/^{86}Sr$ ratios indicated weakening of the South Asian monsoon, which were probably correlated with short-term northern Atlantic climate variability on millennial time scales (Ali et al., 2015).

Before the LGM, sedimentary records at core 12I712 better matched the Intertropical Convergence Zone (ITCZ) migration; when the ITCZ shifted northward and simultaneously the monsoon climate became wetter, more sediments from the G-B Rivers were discharged into the study area, and sediments from the eastern Indian Peninsula decreased (Fig. 8). This finding is in accordance with previous observations and modeling results that indicated that the interhemispheric temperature gradient directly controls the tropical hydrologic cycle and further atmospheric heat transport (Gibbons et al., 2014). In the Arabian Sea, declining rainfall was connected with the northward migration of the ITCZ and the associated summer monsoon pattern (Luckge et al., 2001; Fuchs and Buerkert, 2008). Currently, the ITCZ shifts northward, resulting in more sediments being discharged into the northern Indian Ocean from the southern Indian Peninsula caused by excess rainfall (Yadav, 2013). In the Cariaco Basin, source changes similarly reflected ITCZ migration despite the probable influence of eustatic variations (Riboulleau et al., 2014).

4.4. Modeling sediment supply from the G-B river system

Submarine canyons/channels were concluded to function only during times of sea-level low stand (Weber et al., 1997). Different from the model of turbidity current deposition for the Bengal Fan based on sea-level fluctuation, we build up a new model of sediment transport patterns from the G-B river system controlled by climate variations (Fig. 9). During the Holocene, sediment volume estimates revealed that approximately 30% of the G-B Rivers' load was deposited at the subaqueous delta, and modern sediment is transported off-shelf to the Bengal Fan through the Swatch of No Ground Canyon which is connected the Active Channel with the G-B river system (Kuehl et al., 1997). Turbidity currents, which were confined to the channel and gradually filled it (Weber et al., 1997), were small and probably less frequent; similarly, overflow occurred less frequently (Curray et al., 2003). A study from the distal Bengal Fan also indicated that the sediment deposition by turbidity current activity ceased due to the rapid sea-level rise during the Holocene (Kessarkar et al., 2005). Therefore, deposition occurred within the channel of the middle Bengal Fan, and little or even nearly no turbidity current deposition could reach the lower Bengal Fan (Curray et al., 2003). This finding is in accordance with a modern survey during the southwesterly winds of the monsoon when a warm and saline intermediate water mass is advected northeastward into the BoB up to 14°N, as shown in Fig. 9a (Murty et al., 1992). This observed northward subsurface current in the east of the EICC could carry high-salinity water into the BoB during both the southwest and northeast monsoons (Wijesekera et al., 2015).

However, during heavy sediment supply from the G-B river system when the global climate was cold, slumping and turbidity currents occurred more frequently due to large amounts of fluvial sediments being deposited in the canyon heads or on the slope. When the turbidity currents reached a certain scale, they spilled

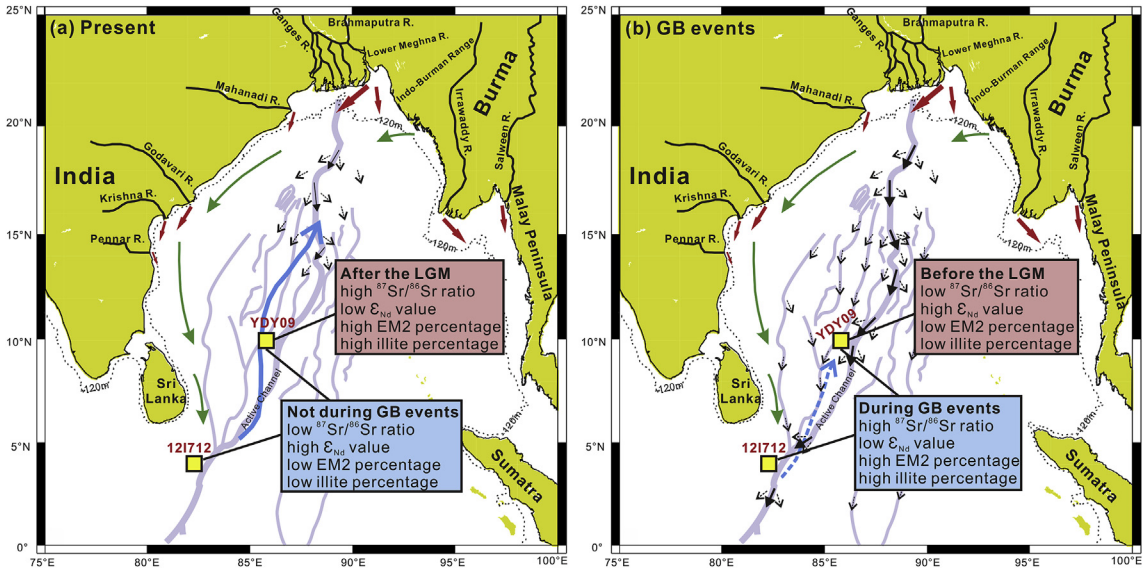

Fig. 9. Map showing dispersal patterns of the G-B river system under (a) present and (b) GB event conditions in the northeastern Indian Ocean. The red and green arrows represent the main dispersal directions when the fluvial sediments were discharged into the BoB. Black solid and dashed arrows denote turbidities and turbidity overflows (including deduced turbidities), respectively, on the Bengal Fan (Curray et al., 2003; Li et al., 2017). Blue solid and dashed arrows symbolize the measured subsurface current (Murty et al., 1992) and deduced deep-water current, respectively. Gray lines denote channels (including Active Channel) developed in the Bengal Fan. Composition changes in the two study cores are shown by comparing stages during GB events with stages not during GB events and periods after the LGM with period before the LGM. (For interpretation of the references to colour in this figure legend, the reader is referred to the Web version of this article.)

over the levee crests and overflow occurred in the Bengal Fan; some sediments were deposited outside the channels to form terminal lobes, and some sediments were deposited within the channels (Curray et al., 2003; Li et al., 2017). These might be caused by weakened deep-water currents, resulting in more G-B river-derived sediments being transported into the study area (Fig. 9b). This finding is confirmed by benthic foraminifera in the central BoB, where the glacial deep-water masses during the LGM remained isolated from the deep waters formed in the North Atlantic (Raza and Ahmad, 2013; Raza et al., 2014). Sedimentary records far north of the equator in the Arabian Sea also indicated that northern extensions of glacial Antarctic Intermediate Water (GAAIW) coincided with reduced thermohaline overturn in the North Atlantic associated with the Heinrich-ice surge events, suggesting that Southern Hemisphere drove intermediate water mass variability (Jung et al., 2009).

In summary, sediments of the G-B river system are characterized by high $^{87}Sr/^{86}Sr$ ratios, low ε_{Nd} values and high illite percentages, together with low smectite percentages (Figs. 6 and 7). Here, we conclude that climate change rather than sea-level fluctuation determined the G-B river sediments discharged into the distal Bengal Fan over the past 50 ka, which is in accordance with records from the Andaman Sea that indicated that variations in the summer monsoon intensity rather than sea-level changes determined clay mineral assemblage fluctuations (Colin et al., 1999). The most noteworthy evidence from the study area is that heavy sediment supply from the G-B river system occurred during the global cold climate events (YD and Heinrich events) rather than just during the low sea-level stand before the LGM (Fig. 8). Moreover, the heavy sediments supplied from the G-B river system were not coarser than those deposited at other times, such as the description by Curray et al. (2003), but in accordance with the peaks of the intermediate fraction (EM2).

5. Conclusions

High-resolution grain size and clay mineralogy combined with Sr and Nd isotope analyses were utilized to explore the relationship between climate change and fine-grained sediment supply from the G-B river system into the Bengal Fan over the past 50 ka. Grain-size analysis reveals that the intermediate end-member represents the flux of distal fluvial particles from the G-B river system, and the fine end-member denotes regional sediment supply of weathered volcanic materials, especially from the eastern Indian Peninsula, while the coarse end-member probably reflects nearby terrigenous input, aeolian input and/or volcanic glass. Sediment provenance based on the clay minerals and Sr–Nd isotopes indicated that the G-B Rivers and eastern Indian rivers (e.g., Godavari and Krishna Rivers) provided most sediments in the two study cores. In the two study cores, heavy terrigenous materials were transported from the G-B Rivers through extensively developed channels, which occurred simultaneously with global cold climate events over the past 50 ka. At core YDY09 inside the BoB, the sediments were primarily derived from the G-B river system in the north. By contrast at core 12I712 outside the BoB, the sediments primarily originated from the eastern Indian rivers. During five G-B events at 50–45 ka (GB5), 42–37 ka (GB4), 31–28.5 ka (GB3), 24–20 ka (GB2) and 14–9 ka (GB1), the sediment supply from the G-B river system reached peak for both cores. In contrast, during other periods, more sediments from eastern India reached the two study cores. In summary, sediments discharged from the G-B Rivers into the distal Bengal Fan were more correlated with climate changes than with global sea-level fluctuations over the past 50 ka, and widely developed channels exposed on the Bengal Fan were important passageways for the G-B river sediments entering the deep-water environments of the Bengal Fan. Meanwhile, there was likely an important transformation of deep-water currents that prevented more sediments of the G-B river system from entering the deep-sea environment at approximately 26 ka, similar to the northeastward flowing subsurface watermass in the BoB.

Acknowledgments

We thank Stephan Steinke and Yun Huang for generating the

chronologies and modeling end-members of the grain-size data for these two cores, and Xuebo Yin for Sr and Nd isotope measurements. We also thank the editor, Ingrid Hendy, Eduardo Garzanti and another anonymous reviewer for their critical comments and suggestions. Core sediment samples were collected on board of R/V "Shiyan 1" implementing the open research cruise NORC 2012-08 supported by NSFC Shiptime Sharing Project. This work was jointly supported by the National Programme on Global Change and Air-Sea Interaction (GASI-GEOGE-06-03), the Innovative Development Fund Projects of Innovation Research Institute on South China Sea Ecological and Environmental Engineering, Chinese Academy of Sciences (ISEE2018PY02), the Strategic Priority Research Program of the Chinese Academy of Sciences (XDA11030103 and XDA11030104), National Natural Science Foundation of China (41676054), the Natural Science Foundation of China-Shandong Joint Fund for Marine Science Research Centers (U1606401) and the Scientific and Technological Innovation Project Financially Supported by Qingdao National Laboratory for Marine Science and Technology (2016ASKJ13).

References

Ahmad, S.M., Babu, G.A., Padmakumari, V.M., Dayal, A.M., Sukhija, B.S., Nagabhushanam, P., 2005. Sr, Nd isotopic evidence of terrigenous flux variations in the Bay of Bengal: implications of monsoons during the last similar to 34,000 years. Geophys. Res. Lett. 32 (22), L22711.

Ahmad, S.M., Padmakumari, V.M., Babu, G.A., 2009. Strontium and neodymium isotopic compositions in sediments from Godavari, Krishna and Pennar rivers. Curr. Sci. 97 (12), 1766–1769.

Ali, S., Hathorne, E.C., Frank, M., Gebregiorgis, D., Stattegger, K., Stumpf, R., Kutterolf, S., Johnson, J.E., Giosan, L., 2015. South Asian monsoon history over the past 60 kyr recorded by radiogenic isotopes and clay mineral assemblages in the Andaman Sea. Geochem. Geophys. Geosyst. 16 (2), 505–521.

Awasthi, N., Ray, J.S., Singh, A.K., Band, S.T., Rai, V.K., 2014. Provenance of the late quaternary sediments in the Andaman Sea: implications for monsoon variability and ocean circulation. Geochem. Geophys. Geosyst. 15 (10), 3890–3906.

Beck, J.W., Zhou, W.J., Li, C., Wu, Z.K., White, L., Xian, F., Kong, X.H., An, Z., 2018. A 550,000-year record of East Asian monsoon rainfall from Be-10 in loess. Science 360, 877–881.

Bejugam, P., Nayak, G.N., 2016a. Source and depositional processes of the surface sediments and their implications on productivity in recent past off Mahanadi to Pennar River mouths, western Bay of Bengal. Palaeogeogr. Palaeoclimatol. Palaeoecol. 483, 58–69.

Bejugam, P., Nayak, G.N., 2016b. Changing depositional environment revealed from sediment components, west of "Swatch of No Ground", northern Bay of Bengal. Arabian J. Geosci. 9 (9), 551.

Biscaye, P.E., 1965. Mineralogy and sedimentation of recent deep-sea clay in Atlantic Ocean and adjacent seas and oceans. Geol. Soc. Am. Bull. 76 (7), 803–832.

Blaauw, M., Christen, J.A., 2011. Flexible paleoclimate age-depth models using an autoregressive gamma process. Bayesian Analysis 6 (3), 457–474.

Carolin, S.A., Cobb, K.M., Lynch-Stieglitz, J., Moerman, J.W., Partin, J.W., Lejau, S., Malang, J., Clark, B., Tuen, A.A., Adkins, J.F., 2016. Northern Borneo stalagmite records reveal West Pacific hydroclimate across MIS 5 and 6. Earth Planet. Sci. Lett. 439, 182–193.

Chandrasekharam, D., Santo, A.P., Capaccioni, B., Vaselli, O., Alam, M.A., Manetti, P., Tassi, F., 2009. Volcanological and petrological evolution of barren Island (Andaman Sea, Indian ocean). J. Asian Earth Sci. 35 (5), 469–487.

Chauhan, O.S., Patil, S.K., Suneethi, J., 2004. Fluvial influx and weathering history of the Himalayas since Last Glacial Maxima - isotopic, sedimentological and magnetic records from the Bay of Bengal. Curr. Sci. 87 (4), 509–515.

Chauhan, O.S., Vogelsang, E., 2006. Climate induced changes in the circulation and dispersal patterns of the fluvial sources during late Quaternary in the middle Bengal Fan. Journal of Earth System Science 115 (3), 379–386.

Clark, P.U., Dyke, A.S., Shakun, J.D., Carlson, A.E., Clark, J., Wohlfarth, B., Mitrovica, J.X., Hostetler, S.W., McCabe, A.M., 2009. The last glacial maximum. Science 325 (5941), 710–714.

Colin, C., Turpin, L., Bertaux, J., Desprairies, A., Kissel, C., 1999. Erosional history of the Himalayan and Burman ranges during the last two glacial-interglacial cycles. Earth Planet. Sci. Lett. 171 (4), 647–660.

Colin, C., Turpin, L., Blamart, D., Frank, N., Kissel, C., Duchamp, S., 2006. Evolution of weathering patterns in the Indo-Burman Ranges over the last 280 kyr: effects of sediment provenance on Sr-87/Sr-86 ratios tracer. Geochem. Geophys. Geosyst. 7, Q03007.

Curray, J.R., Emmel, F.J., Moore, D.G., 2003. The Bengal Fan: morphology, geometry, stratigraphy, history and processes. Mar. Petrol. Geol. 19 (10), 1191–1223.

Datta, D.K., Subramanian, V., 1997. Texture and mineralogy of sediments from the Ganges-Brahmaputra-Meghna river system in the Bengal basin, Bangladesh and their environmental implications. Environ. Geol. 30 (3–4), 181–188.

DiNezio, P.N., Tierney, J.E., 2013. The effect of sea level on glacial Indo-Pacific climate. Nat. Geosci. 6 (6), 485–491.

Ehlert, C., Grasse, P., Frank, M., 2013. Changes in silicate utilisation and upwelling intensity off Peru since the Last Glacial Maximum - insights from silicon and neodymium isotopes. Quat. Sci. Rev. 72, 18–35.

Ehrmann, W., 1998. Implications of late Eocene to early Miocene clay mineral assemblages in McMurdo Sound (Ross Sea, Antarctica) on paleoclimate and ice dynamics. Palaeogeogr. Palaeoclimatol. Palaeoecol. 139 (3–4), 213–231.

Esquevin, J., 1969. Influence de la composition chimique des illites surcristallinite. Bulletin Centre Rechcherche Pau-SNPA 3 (1), 147–153.

Farmer, G.L., Barber, D., Andrews, J., 2003. Provenance of late quaternary ice-proximal sediments in the north atlantic: Nd, Sr and Pb isotopic evidence. Earth Planet. Sci. Lett. 209 (1–2), 227–243.

Fournier, L., Fauquembergue, K., Zaragosi, S., Zorzi, C., Malaize, B., Bassinot, F., Joussain, R., Colin, C., Moreno, E., Leparmentier, F., 2017. The bengal fan: external controls on the Holocene Active Channel turbidite activity. Holocene 27 (6), 900–913.

Fuchs, M., Buerkert, A., 2008. A 20 ka sediment record from the Hajar Mountain range in N-Oman, and its implication for detecting arid-humid periods on the southeastern Arabian Peninsula. Earth Planet. Sci. Lett. 265 (3–4), 546–558.

Garzanti, E., Ando, S., France-Lanord, C., Censi, P., Vignola, P., Galy, V., Lupker, M., 2011. Mineralogical and chemical variability of fluvial sediments 2. Suspended-load silt (Ganga-Brahmaputra, Bangladesh). Earth Planet. Sci. Lett. 302 (1–2), 107–120.

Gherboudj, I., Beegum, S.N., Ghedira, H., 2017. Identifying natural dust source regions over the Middle-East and North-Africa: estimation of dust emission potential. Earth Sci. Rev. 165, 342–355.

Gibbons, F.T., Oppo, D.W., Mohtadi, M., Rosenthal, Y., Cheng, J., Liu, Z.Y., Linsley, B.K., 2014. Deglacial delta O-18 and hydrologic variability in the tropical Pacific and Indian Oceans. Earth Planet. Sci. Lett. 387, 240–251.

Goodbred, S.L., Kuehl, S.A., 1999. Holocene and modern sediment budgets for the Ganges-Brahmaputra river system: evidence for highstand dispersal to flood-plain, shelf, and deep-sea depocenters. Geology 27 (6), 559–562.

Goodbred, S.L., Kuehl, S.A., 2000. Enormous Ganges-Brahmaputra sediment discharge during strengthened early Holocene monsoon. Geology 28 (12), 1083–1086.

Gourlan, A.T., Meynadier, L., Allegre, C.J., Tapponnier, P., Birck, J.L., Joron, J.L., 2010. Northern Hemisphere climate control of the Bengali rivers discharge during the past 4 Ma. Quat. Sci. Rev. 29 (19–20), 2484–2498.

Grand, M.M., Measures, C.I., Hatta, M., Hiscock, W.T., Buck, C.S., Landing, W.M., 2015. Dust deposition in the eastern Indian Ocean: the ocean perspective from Antarctica to the Bay of Bengal. Glob. Biogeochem. Cycles 29 (3), 357–374.

Grootes, P.M., Stuiver, M., White, J.W.C., Johnsen, S., Jouzel, J., 1993. Comparison of oxygen-isotope records from the GISP2 and GRIP Greenland ice cores. Nature 366, 552–554.

Hao, Q.Z., Wang, L., Oldfield, F., Peng, S.Z., Qin, L., Song, Y., Xu, B., Qiao, Y.S., Bloemendal, J., Guo, Z.T., 2012. Delayed build-up of Arctic ice sheets during 400,000-year minima in insolation variability. Nature 490, 393–396.

Huang, C., Zeng, T., Ye, F., Xie, L.H., Wang, Z.B., Wei, G.J., Lo, L., Deng, W.F., Rao, Z.G., 2018. Natural and anthropogenic impacts on environmental changes over the past 7500 years based on the multi-proxy study of shelf sediments in the northern South China Sea. Quat. Sci. Rev. 197, 35–48.

Ismaiel, M., Krishna, K.S., Srinivas, K., Mishra, J., Saha, D., 2017. Internal structure of the 85 degrees E ridge, Bay of Bengal: evidence for multiphase volcanism. Mar. Petrol. Geol. 80, 254–264.

Jacobsen, S.B., Wasserburg, G.J., 1980. Sm-Nd isotopic evolution of chondrites. Earth Planet. Sci. Lett. 50 (1), 139–155.

Jin, C.S., Liu, Q.S., Xu, D.K., Sun, J.M., Li, C.G., Zhang, Y., Han, P., Liang, W.T., 2019. A new correlation between Chinese loess and deep-sea delta O-18 records since the middle Pleistocene. Earth Planet. Sci. Lett. 506, 441–454.

Joussain, R., Colin, C., Liu, Z.F., Meynadier, L., Fournier, L., Fauquembergue, K., Zaragosi, S., Schmidt, F., Rojas, V., Bassinot, F., 2016. Climatic control of sediment transport from the Himalayas to the proximal NE Bengal Fan during the last glacial-interglacial cycle. Quat. Sci. Rev. 148, 1–16.

Joussain, R., Liu, Z.F., Colin, C., Duchamp-Alphonse, S., Yu, Z.J., Moreno, E., Fournier, L., Zaragosi, S., Dapoigny, A., Meynadier, L., 2017. Link between Indian monsoon rainfall and physical erosion in the Himalayan system during the Holocene. Geochem. Geophys. Geosyst. 18 (9), 3452–3469.

Jung, S.J.A., Kroon, D., Ganssen, G., Peeters, F., Ganeshram, R., 2009. Enhanced Arabian Sea intermediate water flow during glacial North Atlantic cold phases. Earth Planet. Sci. Lett. 280, 220–228.

Kessarkar, P.M., Rao, V.P., Ahmad, S.M., Patil, S.K., Kumar, A.A., Babu, G.A., Chakraborty, S., Rajan, R.S., 2005. Changing sedimentary environment during the late quaternary: sedimentological and isotopic evidence from the distal bengal fan. Deep Sea Res. Oceanogr. Res. Pap. 52 (9), 1591–1615.

Kolla, V., Moore, D.G., Curray, J.R., 1976. Recent bottom-current activity in the deep western Bay of Bengal. Mar. Geol. 21 (4), 255–270.

Konert, M., Vandenberghe, 1997. Comparison of laser grain size analysis with pipette and sieve analysis: a solution for the underestimation of the clay fraction. Sedimentology 44 (3), 523–535.

Kottke, B., Schwenk, T., Breitzke, M., Wiedicke, M., Kudrass, H.R., Spiess, V., 2003. Acoustic facies and depositional processes in the upper submarine canyon Swatch of No Ground (Bay of Bengal). Deep Sea Res. Part II Top. Stud. Oceanogr. 50 (5), 979–1001.

Kuehl, S.A., Levy, B.M., Moore, W.S., Allison, M.A., 1997. Subaqueous delta of the

Ganges-Brahmaputra river system. Mar. Geol. 144 (1–3), 81–96.
Li, J.R., Liu, S.F., Shi, X.F., Feng, X.L., Fang, X.S., Cao, P., Sun, X.Q., Ye, W.X., Khokiattiwong, S., Kornkanitnan, N., 2017. Distributions of clay minerals in surface sediments of the middle Bay of Bengal: source and transport pattern. Cont. Shelf Res. 145, 59–67.
Li, J.R., Liu, S.F., Shi, X.F., Zhang, H., Fang, X.S., Chen, M.T., Cao, P., Sun, X.Q., Ye, W.X., Wu, K.K., 2018. Clay minerals and Sr-Nd isotopic composition of the Bay of Bengal sediments: implications for sediment provenance and climate control since 40 ka. Quat. Int. 493, 50–58.
Licht, A., France-Lanord, C., Reisberg, L., Fontaine, C., Soe, A.N., Jaeger, J.J., 2013. A palaeo Tibet-Myanmar connection? Reconstructing the Late Eocene drainage system of central Myanmar using a multi-proxy approach. J. Geol. Soc. (Lond.) 170 (6), 929–939.
Liu, J., Steinke, S., Vogt, C., Mohtadi, M., De Pol-Holz, R., Hebbeln, D., 2017. Temporal and spatial patterns of sediment deposition in the northern South China Sea over the last 50,000 years. Palaeogeogr. Palaeoclimatol. Palaeoecol. 465, 212–224.
Liu, Z., Wang, H., Hantoro, W.S., Sathiamurthy, E., Colin, C., Zhao, Y.L., Li, J.R., 2012. Climatic and tectonic controls on chemical weathering in tropical southeast asia (Malay Peninsula, Borneo, and Sumatra). Chem. Geol. 291, 1–12.
Luckge, A., Doose-Rolinski, H., Khan, A.A., Schulz, H., von Rad, U., 2001. Monsoonal variability in the northeastern Arabian Sea during the past 5000 years: geochemical evidence from laminated sediments. Palaeogeogr. Palaeoclimatol. Palaeoecol. 167 (3–4), 273–286.
Lupker, M., France-Lanord, C., Galy, V., Lave, J., Kudrass, H., 2013. Increasing chemical weathering in the himalayan system since the last glacial maximum. Earth Planet. Sci. Lett. 365, 243–252.
Mazumdar, A., Kocherla, M., Carvalho, M.A., Peketi, A., Joshi, R.K., Mahalaxmi, P., Joao, H.M., Jisha, R., 2015. Geochemical characterization of the Krishna-Godavari and Mahanadi offshore basin (Bay of Bengal) sediments: a comparative study of provenance. Mar. Petrol. Geol. 60, 18–33.
Milliman, J.D., Farnswork, K.L., 2011. River Discharge to the Coastal Ocean: a Global Synthesis. Cambridge Univ. Press, New York.
Murty, V.S.N., Sarma, Y.V.B., Rao, D.P., Murty, C.S., 1992. Water characteristics, mixing and circulation in the Bay of bengal during southwest monsoon. J. Mar. Res. 50 (2), 207–228.
Nagasundaram, M., Achyuthan, H., Ahmad, S.M., 2014. Monsoonal changes inferred from the middle to late Holocene sediments off landfall Island, north andaman. Arabian Journal of Geosciences 7 (9), 3513–3523.
Paterson, G.A., Heslop, D., 2015. New methods for unmixing sediment grain size data. Geochem. Geophys. Geosyst. 16 (12), 4494–4506.
Phillips, S.C., Johnson, J.E., Underwood, M.B., Guo, J.H., Giosan, L., Rose, K., 2014. Long-timescale variation in bulk and clay mineral composition of Indian continental margin sediments in the Bay of Bengal, Arabian Sea, and Andaman Sea. Mar. Petrol. Geol. 58, 117–138.
Prins, M., Postma, G., Weltje, G.J., 2000. Controls on terrigenous sediment supply to the Arabian Sea during the late Quaternary: the Makran continental slope. Mar. Geol. 169 (3–4), 351–371.
Raman, C.V., Rao, G.K., Reddy, K.S.N., Ramesh, M.V., 1995. Clay mineral distributions in the continental-shelf sediments between the Ganges mouths and madras, east-coast of India. Cont. Shelf Res. 15 (14), 1773–1793.
Ramaswamy, V., Kumar, B.V., Parthiban, G., Ittekkot, V., Nair, R.R., 1997. Lithogenic fluxes in the Bay of Bengal measured by sediment traps. Deep Sea Res. Oceanogr. Res. Pap. 44 (5), 793–810.
Ramaswamy, V., Rao, P.S., Rao, K.H., Thwin, S., Rao, N.S., Raiker, V., 2004. Tidal influence on suspended sediment distribution and dispersal in the northern Andaman Sea and Gulf of Martaban. Mar. Geol. 208, 33–42.
Rao, P.S., Ramaswamy, V., Thwin, S., 2005. Sediment texture, distribution and transport on the Ayeyarwady continental shelf, Andaman Sea. Mar. Geol. 216, 239–247.
Raza, T., Ahmad, S.M., 2013. Surface and deep water variations in the northeast Indian Ocean during 34-6 ka BP: evidence from carbon and oxygen isotopes of fossil foraminifera. Quat. Int. 298, 37–44.
Raza, T., Ahmad, S.M., Sahoo, M., Banerjee, B., Bal, I., Dash, S., Suseela, G., Mukherjee, I., 2014. Hydrographic changes in the southern Bay of Bengal during the last similar to 65,000 y inferred from carbon and oxygen isotopes of foraminiferal fossil shells. Quat. Int. 333, 77–85.
Reddy, N.P.C., Rao, K.M., 2001. Heavy sediment influx during early Holocene: Inference from clay mineral studies in a core from the Western Bay of Bengal. Curr. Sci. 81, 1361–1364.
Reimer, P.J., Bard, E., Bayliss, A., Beck, J.W., Blackwell, P.G., Ramsey, C.B., Buck, C.E., Cheng, H., Edwards, R.L., Friedrich, M., 2013. Intcal13 and Marine13 radiocarbon age calibration curves 0-50,000 years cal BP. Radiocarbon 55 (4), 1869–1887.
Riboulleau, A., Bout-Roumazeilles, V., Tribovillard, N., 2014. Controls on detrital sedimentation in the Cariaco Basin during the last climatic cycle: insight from clay minerals. Quat. Sci. Rev. 94, 62–73.
Rodolfo, 1969. Sediments of the andaman basin, northeastern Indian ocean. Mar. Geol. 7 (5), 371–402.
Rogers, K.G., Goodbred, S.L., Khan, S.R., 2015. Shelf-to-canyon connections: transport-related morphology and mass balance at the shallow-headed, rapidly aggrading Swatch of No Ground (Bay of Bengal). Mar. Geol. 369, 288–299.
Sarma, V., Kumari, V.R., Srinivas, T.N.R., Krishna, M.S., Ganapathi, P., Murty, V.S.N., 2018. East India Coastal Current controls the dissolved inorganic carbon in the coastal Bay of Bengal. Mar. Chem. 205, 37–47.
Schott, F.A., McCreary, J.P., 2001. The monsoon circulation of the Indian Ocean. Prog. Oceanogr. 51 (1), 1–123.
Segall, M.P., Kuehl, S.A., 1992. Seidmentary processes on the bengal continental-shelf as revealed by clay-size mineralogy. Cont. Shelf Res. 12 (4), 517–541.
Shankar, D., Vinayachandran, P.N., Unnikrishnan, A.S., 2002. The monsoon currents in the north Indian Ocean. Prog. Oceanogr. 52 (1), 63–120.
Stenni, B., Jouzel, J., Masson-Delmotte, V., Roghlisberger, R., Castellano, E., Cattani, O., Falourd, S., Johnsen, S.J., Longinelli, A., Sachs, J.P., 2004. A late-glacial high-resolution site and source temperature record derived from the EPICA Dome C isotope records (East Antarctica). Earth Planet. Sci. Lett. 217 (1–2), 183–195.
Stewart, J.A., Gutjahr, M., James, R.H., Anand, P., Wilson, P.A., 2016. Influence of the Amazon River on the Nd isotope composition of deep water in the western equatorial Atlantic during the Oligocene-Miocene transition. Earth Planet. Sci. Lett. 454, 132–141.
Stoll, H.M., Vance, D., Arevalos, A., 2007. Records of the Nd isotope composition of seawater from the Bay of Bengal: implications for the impact of Northern Hemisphere cooling on ITCZ movement. Earth Planet. Sci. Lett. 255 (1–2), 213–228.
Symphonia, K.T., Nathan, D.S., 2018. Geochemistry and distribution of sediments in the East Indian shelf, SW Bay of Bengal: implications on weathering, transport and depositional environment. Journal of Earth System Science 127 (7), 18.
Tiwari, M., Ramesh, R., Somayajulu, B.L.K., Jull, A.J.T., Burr, G.S., 2005. Early deglacial (similar to 19-17 ka) strengthening of the northeast monsoon. Geophys. Res. Lett. 32 (19), 4.
Tripathy, G.R., Singh, S.K., Bhushan, R., Ramaswamy, V., 2011. Sr-Nd isotope composition of the Bay of Bengal sediments: impact of climate on erosion in the Himalaya. Geochem. J. 45 (3), 175–186.
Unger, D., Ittekkot, V., Schafer, P., Tiemann, J., Reschke, S., 2003. Seasonality and interannual variability of particle fluxes to the deep Bay of Bengal: influence of riverine input and oceanographic processes. Deep Sea Res. Part II Top. Stud. Oceanogr. 50 (5), 897–923.
Venkatar, K., Biscaye, P.E., 1973. Clay mineralogy and sedimentation in eastern Indian-ocean. Deep-Sea Res. 20 (8), 727–738.
Warren, B.A., 1981. Transindian hydrographic section at lat 18-Degrees-s -property distributions and circulation in the south Indian-ocean. Deep-Sea Res. Part a 28 (8), 759–788.
Weber, M.E., Wiedicke, M.H., Kudrass, H.R., Hubscher, C., Erlenkeuser, H., 1997. Active growth of the Bengal Fan during sea-level rise and highstand. Geology 25 (4), 315–318.
Weber, M.E., Lantzsch, H., Dekens, P., Das, S.K., Reilly, B.T., Martos, Y.M., Meyer-Jacob, C., Agrahari, S., Ekblad, A., Titschack, J., Holmes, B., Wolfgramm, P., 2018. 200,000 years of monsoonal history recorded on the lower Bengal Fan - strong response to insolation forcing. Glob. Planet. Chang. 166, 107–119.
Weber, M.E., Reilly, B.T., 2018. Hemipelagic and turbiditic deposits constrain lower Bengal Fan depositional history through Pleistocene climate, monsoon, and sea level transitions. Quat. Sci. Rev. 199, 159–173.
Wijesekera, H.W., Jensen, T.G., Jarosz, E., Teague, W.J., Metzger, E.J., Wang, D.W., Jinadasa, S.U.P., Arulananthan, K., Centurioni, L.R., Fernando, H.J.S., 2015. Southern Bay of Bengal currents and salinity intrusions during the northeast monsoon. Journal of Geophysical Research-Oceans 120 (10), 6897–6913.
Yadav, R.K., 2013. Emerging role of Indian ocean on Indian northeast monsoon. Clim. Dyn. 41 (1), 105–116.
Yu, Z.J., Wan, S.M., Colin, C., Song, L.N., Zhao, D.B., Huang, J., Sun, H.J., Xu, Z.J., Li, A.C., Li, T.G., 2018. ENSO-like modulated tropical Pacific climate changes since 2.36 Myr and its implication for the Middle Pleistocene Transition. Geochem. Geophys. Geosyst. 19, 415–426.
Zonneveld, K.A.F., Ganssen, G., Troelstra, S., Versteegh, G.T.M., Visscher, H., 1997. Mechanisms forcing abrupt fluctuations of the Indian Ocean summer monsoon during the last deglaciation. Quat. Sci. Rev. 16, 187–201.